AAS 20-644

HELIOCENTRIC ACCESS FROM CISLUNAR SPACE WITHIN THE CONTEXT OF THE BICIRCULAR RESTRICTED FOUR-BODY PROBLEM

Kenza Boudad[*], Kathleen Howell[†], Diane Davis[‡]

In the next decades, multiple missions are proposed or planned to originate in the vicinity of the Moon and be delivered to heliocentric space, such as servicing missions to the Nancy Roman or the James Webb Space Telescopes, as well as departures from Gateway to other interplanetary destinations. The Earth-Moon-Sun transit dynamics are complex, primarily influenced by the Earth and the Moon in cislunar space; the gravitational influence of the Sun becomes significant after departure from the Earth-Moon vicinity. The current investigation leverages an Earth-Moon-Sun-spacecraft four-body model, the Bicircular Restricted Four-Body Problem, including dynamical structures in this regime such as periodic orbits and manifolds to design low-energy transfers from the cislunar space to the heliocentric orbits near the Sun-Earth L_2 portal.

INTRODUCTION

Transit between cislunar space and the region near the Sun-Earth L_2 libration point presents many interesting opportunities. The Gateway facility in cislunar space, for example, is planned to serve as a stepping stone for missions to various destinations in the solar system. In addition, the James Webb Space Telescope (JWST) is planned to launch in 2021 to a Sun-Earth L_2 halo or Lissajous orbit, while the Nancy Roman Space Telescope (NRST, previously named WFIRST) is scheduled to arrive in a Sun-Earth L_2 quasihalo in the mid 2020s. The JWST investigation is focused on a study of the various phases in the history of the universe, from the luminous glows originating from the time of the Big Bang to the most recent evolution of the solar system. The NRST's observations aim to answer fundamental questions about the expansion of the universe and exoplanets. Note that missions for servicing observatories such as JWST and NRST are likely to be required during their lifetime. Ross and Lo[1] demonstrate that transfers to the Sun-Earth L_2 libration point from the Earth-Moon L_1 libration point exist for a relatively low cost: 14 m/s and 20 days of flight time, in contrast to 3,200 m/s and 3 months of travel time when the transfer is initiated from a 200 km parking orbit around the Earth. The current reference orbit for the Gateway facility is the 9:2 synodic resonant Near Rectilinear Halo Orbit (NRHO), a member of a family of halo orbits emanating from the Earth-Moon L_2 libration point.[2] The current analysis extends previous work by Folta and Webster[3] by investigating the transfer dynamics between the Earth-Moon L_2 region and the Sun-Earth L_2 vicinity, and offers low-energy transfer strategies between cislunar space and the Sun-Earth portal

[*]Ph.D. Student, School of Aeronautics and Astronautics, Purdue University, West Lafayette, IN 47907; kboudad@purdue.edu

[†]Hsu Lo Distinguished Professor of Aeronautics and Astronautics, School of Aeronautics and Astronautics, Purdue University, West Lafayette, IN 47907; howell@purdue.edu

[‡]Principal Systems Engineer, a.i.solutions, Inc., 2224 Bay Area Blvd, Houston TX 77058; diane.davis@ai-solutions.com

to heliocentric space. This investigation leverages an Earth-Moon-Sun-spacecraft four-body model, the Bicircular Restricted Four-Body Problem, including dynamical structures in this regime such as periodic orbits and manifolds to design low-energy transfers from cislunar space to the heliocentric orbits near the Sun-Earth $\underline{L_2}$ portal.

DYNAMICAL MODELS

Two dynamical models are employed in this investigation. The Circular Restricted Three-Body Problem (CR3BP)[4] is an autonomous model approximating the Earth-Moon system dynamics. The Bicircular Restricted Four-Body Problem (BCR4BP)[5–7] is a time-dependent, periodic model describing the motion of a particle in the Earth-Moon-Sun regime. The BCR4BP is an intermediate step between the CR3BP and a higher-fidelity, time-dependent, non-periodic ephemeris model.

The Circular Restricted 3-Body Problem

In the CR3BP, the motion of a spacecraft of negligible mass is subject to the influence of two primary gravitational bodies, for example, the Earth and the Moon. The model assumes that the two primaries are point masses in circular orbits about their common center of mass. The motion of the spacecraft under the influence of the two primaries is described relative to a rotating frame moving at a fixed rate consistent with the circular rotation of the primaries. By convention, the differential equations governing the CR3BP are nondimensionalized. The characteristic quantities employed include: (i) the Earth-Moon distance; (ii) the sum of the primary masses; (iii) a characteristic time such that the nondimensional gravitational constant $\tilde{G}$ equals unity. The nondimensional equations of motion are then

$$\ddot{x} \;\; = 2\dot{y} + \tfrac{\partial U^*}{\partial x}, \quad \ddot{y} \;\; = -2\dot{x} + \tfrac{\partial U^*}{\partial y}, \quad \ddot{z} \;\; = \tfrac{\partial U^*}{\partial z} \tag{1}$$

where x, y, z (respectively, $\dot{x}, \dot{y}, \dot{z}$) are the position (respectively, the velocity) components of the spacecraft expressed in the Earth-Moon rotating coordinates and derivatives as viewed by an observer in the rotating frame. The associated pseudo-potential U^* is defined as

$$U^* = \frac{1}{2}(x^2 + y^2) + \frac{\mu}{r_{\text{e-sc}}} + \frac{1-\mu}{r_{\text{m-sc}}} \tag{2}$$

The quantities $r_{\text{e-sc}}$ and $r_{\text{m-sc}}$ are the distances between the spacecraft and the primaries, and $\mu = {m_{\text{m}}}/{(m_{\text{e}}+m_{\text{m}})}$ is the mass parameter for the Earth-Moon CR3BP system.

The equations of motion in the CR3BP do not admit a closed-form solution. However, five equilibrium solutions, the libration points, exist and are denoted L_1 through L_5. Stable and unstable orbits in families, such as the L_2 halo family, exist in the CR3BP. The CR3BP allows a single integral of the motion, the Jacobi constant, evaluated as

$$C = 2U^* - \left(\dot{x}^2 + \dot{y}^2 + \dot{z}^2\right) \tag{3}$$

This energy-like quantity limits the motion of the spacecraft to regions where the magnitude of the rotating velocity is real and not a complex quantity. These regions are bounded by Zero Velocity Surfaces (ZVSs). For values of the Jacobi constant greater than the one associated with the L_1 libration point, the ZVSs form two closed regions around each of the primaries. As the energy along the spacecraft trajectory increases, the value of the Jacobi constant decreases until, at the L_1 value, the ZVSs open at the L_1 libration point, and the spacecraft is able to move from the vicinity of one primary to the other. Similarly, when the value of the Jacobi constant decreases

to the value associated with L_2, the ZVSs open at L_2 allowing escape beyond the vicinity of the primaries entirely. For a spacecraft orbiting in one of the selected NRHOs, the CR3BP is a good approximation for the behavior of the trajectory.

The Bicircular Restricted 4-Body Problem

In scenarios where the gravitational influence of the Sun is non-negligible, a higher-fidelity model is necessary to accurately describe the spacecraft behavior. The BCR4BP incorporates the gravitational effect of three massive bodies, for instance, the Earth, the Moon and the Sun, on the motion of a spacecraft.[5–7] The mass of the spacecraft is assumed to be negligible in comparison to the masses of the other bodies. In this model, the Earth and the Moon are assumed to move in circular orbits around their common barycenter, denoted B_1, while the Sun and B_1 move in circular orbits with respect to the Earth-Moon-Sun barycenter, labeled B_2, as denoted in Figure 1. The BCR4BP is not a coherent model: the perturbing acceleration from the Sun does not influence the motion of the Earth and the Moon, thus, the motion of the Moon is not a solution to the Sun-Earth CR3BP. Coherent bicircular models have been investigated previously,[8] but are not necessary in this analysis. The equations of the motion in the CR3BP, in Eq. (1), are extended to include the solar gravitational influence as follows,

$$\ddot{x} = 2\dot{y} + \frac{\partial \Upsilon^*}{\partial x}, \quad \ddot{y} = -2\dot{x} + \frac{\partial \Upsilon^*}{\partial y}, \quad \ddot{z} = \frac{\partial \Upsilon^*}{\partial z} \tag{4}$$

where Υ^* is the pseudo-potential function in the BCR4BP and evaluated as

$$\Upsilon^* = U^* + \frac{\mu_\mathrm{s}}{r_\mathrm{s\text{-}sc}} - \frac{\mu_\mathrm{s}}{a_\mathrm{s}^3}(x_\mathrm{s}x + y_\mathrm{s}y + z_\mathrm{s}z) \tag{5}$$

Then, $\mu_\mathrm{s} = \frac{m_\mathrm{s}}{m_\mathrm{e}+m_\mathrm{m}}$ is the nondimensional mass of the Sun and $a_\mathrm{s} = \frac{r_\mathrm{s}}{r_\mathrm{e\text{-}m}}$ is the nondimensional distance between the Earth-Moon barycenter and the Sun. Note that this adaptation of the BCR4BP assumes the Sun moves in the Earth-Moon plane of motion. The variables $x_\mathrm{s}, y_\mathrm{s}, z_\mathrm{s}$ are the position components of the Sun, originating at B_1, and expressed in terms of the Earth-Moon rotating frame,

$$\begin{bmatrix} x_\mathrm{s} \\ y_\mathrm{s} \\ z_\mathrm{s} \end{bmatrix} = a_\mathrm{s} \begin{bmatrix} \cos(\theta) \\ \sin(\theta) \\ 0 \end{bmatrix} = \begin{bmatrix} \cos(-\omega\, t + \theta_0) \\ \sin(-\omega\, t + \theta_0) \\ 0 \end{bmatrix} \tag{6}$$

where the Sun angle θ is measured from the rotating $\hat{x}$ axis to the Sun position vector as defined in Figure 1, and $\omega = 0.9253$ is the magnitude of the nondimensional angular velocity of the Sun as viewed in the Earth-Moon rotating frame. This angular velocity is computed as the difference between the nondimensional mean motion of the Sun in the inertial frame centered at the Earth-Moon barycenter, that is, $n_S = \sqrt{(1+\mu_\mathrm{s})/a_\mathrm{s}^3}$, and the nondimensional mean motion of the Earth-Moon system with respect to the same observer, n, that is, the value one. Observe that the independent time variable, t, explicitly appears in the BCR4BP pseudo-potential through the Sun terms. Therefore, the BCR4BP is time-dependent and does not admit an integral of the motion. However, a scaled version of the Hamiltonian value is defined to be consistent with the Jacobi constant in the CR3BP, i.e.,

$$H(\theta) = 2\Upsilon^* - \left(\dot{x}^2 + \dot{y}^2 + \dot{z}^2\right) \tag{7}$$

Note that the Hamiltonian value is a function of the Sun angle θ, and thus, a function of the independent time variable. Equations (4) to (7) describe the Earth-Moon-Sun BCR4BP as defined in the Earth-Moon rotating frame.

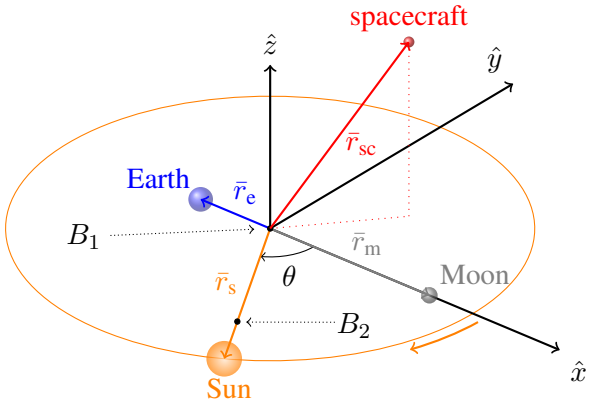

Figure 1. BCR4BP in the Earth-Moon rotating frame.

In scenarios where the spacecraft departs the Earth-Moon vicinity, its trajectory may be more insightful when represented in the Sun-B_1 rotating frame. The BCR4BP equations of motion are, therefore, derived in this frame. In the Sun-B_1 rotating frame, the Sun and B_1 are fixed, while the Earth and the Moon are in circular orbits about their barycenter B_1, as illustrated in Figure 2. The Sun-B_1 rotating frame is centered at B_2. The $\underline{\hat{x}}$-axis is directed from the Sun to B_1, the $\underline{\hat{z}}$ direction is aligned with the Sun-B_1 orbital angular momentum direction, and $\underline{\hat{y}}$ completes the right-handed orthogonal coordinate triad. (Note that underlined variables denote quantities in the Sun-B_1 rotating frame, while non-underlined variables describe quantities in the Earth-Moon rotating frame). In terms of the Sun-B_1 rotating frame, the positions of the Earth and the Moon are uniquely described by the Moon angle, defined as the angle between the rotating $\underline{\hat{x}}$ axis and the position vector from B_1 to Moon, labeled $\underline{\bar{r}}_{B_1\mathrm{m}}$. The equations of motion for the BCR4BP in the Sun-B_1 rotating frame are derived as,

$$\underline{\ddot{x}} = 2\underline{\dot{y}} + \frac{\partial \underline{\Upsilon}^*}{\partial \underline{x}}, \quad \underline{\ddot{y}} = -2\underline{\dot{x}} + \frac{\partial \underline{\Upsilon}^*}{\partial \underline{y}}, \quad \underline{\ddot{z}} = \frac{\partial \underline{\Upsilon}^*}{\partial \underline{z}} \tag{8}$$

where $\underline{\Upsilon^*}$ is the pseudo-potential function defined in the Sun-B_1 rotating frame,

$$\underline{\Upsilon}^* = \frac{1}{2}(\underline{x}^2 + \underline{y}^2) + \frac{1 - \frac{1}{\mu_s+1}}{\underline{r}_{\text{s-sc}}} + \frac{\frac{1}{\mu_s+1}(1-\mu)}{\underline{\bar{r}}_{\text{e-sc}}} + \frac{\frac{\mu}{\mu_s+1}}{\underline{r}_{\text{m-sc}}} \tag{9}$$

The equations of motion in the BCR4BP as formulated in the Sun-B_1 rotating frame, in Eq. (8), represent the same dynamics as the equations of motion for the BCR4BP in the Earth-Moon rotating frame, in Eq. (4). Consistent with the equations of motion in the CR3BP and the equations of motion for the BCR4BP as formulated in the Earth-Moon rotating frame, the equations of motion describing the BCR4BP dynamics in the Sun-B_1 rotating frame are nondimensionalized. The characteristic quantities employed include: (i) the Sun-B_1 distance; (ii) the sum of the Sun, Earth and Moon masses; (iii) a characteristic time such that the nondimensional gravitational constant $\underline{\tilde{G}}$ equals unity. The position of the Earth and the Moon with respect to the system barycenter, B_2, are then

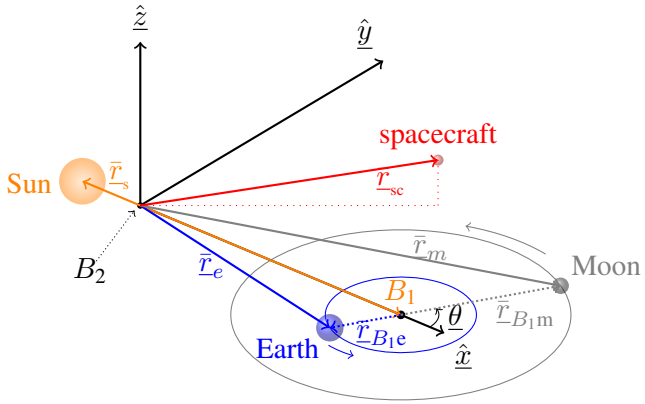

Figure 2. BCR4BP in the Sun-B_1 rotating frame.

defined as,

$$\begin{aligned}\bar{\underline{r}}_e &= \bar{\underline{r}}_{B_1} + \bar{\underline{r}}_{B_1\mathrm{e}} = \begin{bmatrix} 1-\frac{1}{\mu_\mathrm{s}+1} \\ 1-\frac{1}{\mu_\mathrm{s}+1} \\ 0 \end{bmatrix} + \begin{bmatrix} -\frac{\mu}{a_\mathrm{s}}\cos(\underline{\theta}) \\ -\frac{\mu}{a_\mathrm{s}}\sin(\underline{\theta}) \\ 0 \end{bmatrix} \\ \bar{\underline{r}}_m &= \bar{\underline{r}}_{B_1} + \bar{\underline{r}}_{B_1\mathrm{m}} = \begin{bmatrix} 1-\frac{1}{\mu_\mathrm{s}+1} \\ 1-\frac{1}{\mu_\mathrm{s}+1}+ \\ 0 \end{bmatrix} + \begin{bmatrix} \frac{1-\mu}{a_\mathrm{s}}\cos(\underline{\theta}) \\ \frac{1-\mu}{a_\mathrm{s}}\sin(\underline{\theta}) \\ 0 \end{bmatrix}\end{aligned} \tag{10}$$

where $\underline{\theta} = \pi - \theta = \underline{\omega}t + \underline{\theta}_0$ is the Moon angle, and $\underline{\omega} = \frac{\omega}{1-\omega}$ is the nondimensional angular rate of the Earth and the Moon in their motion around their common barycenter B_1. Alignment of the Sun, Earth, and Moon occurs every synodic period, that is, about 29.5 days. Similar to the BCR4BP formulated in the Earth-Moon rotating frame, the Sun-B_1 BCR4BP is a non-autonomous, periodic system. Consistent with Eq. (7), a scaled Hamiltonian value is defined in the Sun-B_1 rotating frame,

$$\underline{H}(\underline{\theta}) = 2\underline{\Upsilon^*} - \left(\dot{\underline{x}}^2 + \dot{\underline{y}}^2 + \dot{\underline{z}}^2\right) \tag{11}$$

Note that this value is a function of the epoch, i.e., the Moon angle $\underline{\theta}$. The equations of motion for the BCR4BP as viewed in the Earth-Moon frame, in Eq. (4), and the formulation in the Sun-B_1 rotating frame, in Eq. (8), describe the same dynamical system. Thus, trajectory design in the BCR4BP leverages two sets of differential equations, i.e., Eq. (4) and Eq. (8), as well as the rotation matrices to transform states from one frame to the other. The BCR4BP is a versatile dynamical model for trajectory design in the Earth-Moon-Sun multi-body regime.

SYNODIC RESONANT ORBITS

Periodic orbits in the CR3BP are solutions that precisely repeat in all six position and velocity states over every period. Previous contributions demonstrate that an infinite number of periodic orbits exist in the CR3BP.[9,10] The BCR4BP is formulated to represent a time-dependent, periodic system. Therefore, only isolated periodic orbits with specific periods exist rather than families with periods that continuously vary.[11] While CR3BP periodic solutions only require periodicity in 6 states, periodic solutions in the BCR4BP require an additional condition: the orientation of the primaries must also repeat with the solar cycle along the orbit.[5,12] Thus, the period for any periodic solution in the BCR4BP is a multiple of the Earth-Moon-Sun period, that is, the synodic period.

Periodic orbits in the BCR4BP are produced by leveraging the corresponding synodic resonant orbit in the CR3BP. Previous contributions include the development of an expanded continuation process to transition periodic solutions between the Earth-Moon CR3BP and the BCR4BP as formulated in the Earth-Moon rotating frame.[5,6,13] This investigation introduces a continuation process between the Sun-B_1 CR3BP and the BCR4BP as formulated in the Sun-B_1 rotating frame. Note that the Sun-B_1 CR3BP is also the representation of a CR3BP where the second body is a fictitious body located at the Earth-Moon barycenter and with mass equal to the sum of the masses of the Earth and the Moon.[14] To transition between the Sun-B_1 CR3BP and the BCR4BP as formulated in the Sun-B_1 rotating frame, the relative positions of the Earth and the Moon with respect to their common barycenter B_1 is varied. The continuation parameter, γ, is introduced and Equation (10) is rewritten as,

$$\begin{aligned}
\bar{\underline{r}}_e &= \bar{\underline{r}}_{B_1} + \gamma\, \bar{\underline{r}}_{B_1\mathrm{e}} = \begin{bmatrix} 1 - \frac{1}{\mu_\mathrm{s}+1} \\ 1 - \frac{1}{\mu_\mathrm{s}+1} \\ 0 \end{bmatrix} + \gamma \begin{bmatrix} -\frac{\mu}{a_\mathrm{s}} \cos(\underline{\theta}) \\ -\frac{\mu}{a_\mathrm{s}} \sin(\underline{\theta}) \\ 0 \end{bmatrix} \\
\bar{\underline{r}}_m &= \bar{\underline{r}}_{B_1} + \gamma\, \bar{\underline{r}}_{B_1\mathrm{m}} = \begin{bmatrix} 1 - \frac{1}{\mu_\mathrm{s}+1} \\ 1 - \frac{1}{\mu_\mathrm{s}+1} + \\ 0 \end{bmatrix} + \gamma \begin{bmatrix} \frac{1-\mu}{a_\mathrm{s}} \cos(\underline{\theta}) \\ \frac{1-\mu}{a_\mathrm{s}} \sin(\underline{\theta}) \\ 0 \end{bmatrix}
\end{aligned} \tag{12}$$

When γ is equal to zero, $\bar{\underline{r}}_e = \bar{\underline{r}}_m = \bar{\underline{r}}_{B_1}$, i.e., the Earth and the Moon are located at B_1, creating a fictitious body of mass equal to the sum of the masses of the Earth and the Moon. This case corresponds to the Sun-B_1 CR3BP. When γ is equal to one, Equation (10) and Equation (12) are identical, and the BCR4BP, as expressed in the Sun-B_1 rotating frame, emerges. For instance, consider the transition of the 2:17 $\underline{\mathrm{L}}_2$ synodic resonant Lyapunov orbit from the CR3BP to the BCR4BP in Figure 3. The minimal period of the 2:17 resonant Lyapunov orbit in the CR3BP is $17/2$, or 8.5 synodic periods. However, the period associated with periodic solutions in the BCR4BP must be equal to an integer multiple of the synodic period.[5] Thus, two revolutions of the CR3BP orbit are stacked to form the initial guess for the BCR4BP periodic orbit. The transition process to an orbit in the BCR4BP includes a targeting scheme.[13] The trajectory is discretized into patch points, and a parallel-shooting scheme[15] is employed to mitigate the potential convergence issues arising from the long period of the orbit. At each step, represented by the evolving value of the continuation parameter, γ, the solution is propagated and corrected for continuity between consecutive patch points as well as for periodicity. Once a solution for a given γ value is computed, it is employed as the initial guess for the next step in the continuation procedure. For the example in Figure 3(a), 50 equally-spaced steps between $\gamma = 0$ and $\gamma = 1$ are introduced, and the converged, periodic solution for each step is plotted. The solution corresponding to $\gamma = 1$, colored in black in Figure 3(b), reflects the Earth-Moon-Sun BCR4BP periodic solution. In this investigation, each BCR4BP periodic orbit is constructed using this method, in which a synodic resonant CR3BP orbit serves as the initial guess for a continuation process with the relative distance of the Earth and the Moon as the continuation parameter.

Synodic Resonant Halo Orbits

The $\underline{\mathrm{L}}_1$, $\underline{\mathrm{L}}_2$, and $\underline{\mathrm{L}}_3$ halo families are comprised of three-dimensional periodic orbits in the CR3BP.[16] The halo family of orbits bifurcates from each family of planar Lyapunov orbits associated with the collinear libration points. The halo orbits are mirrored across the $\underline{x}$-$\underline{y}$ plane; a northern family member possesses a positive $\underline{z}$ component over the majority of each orbit, while

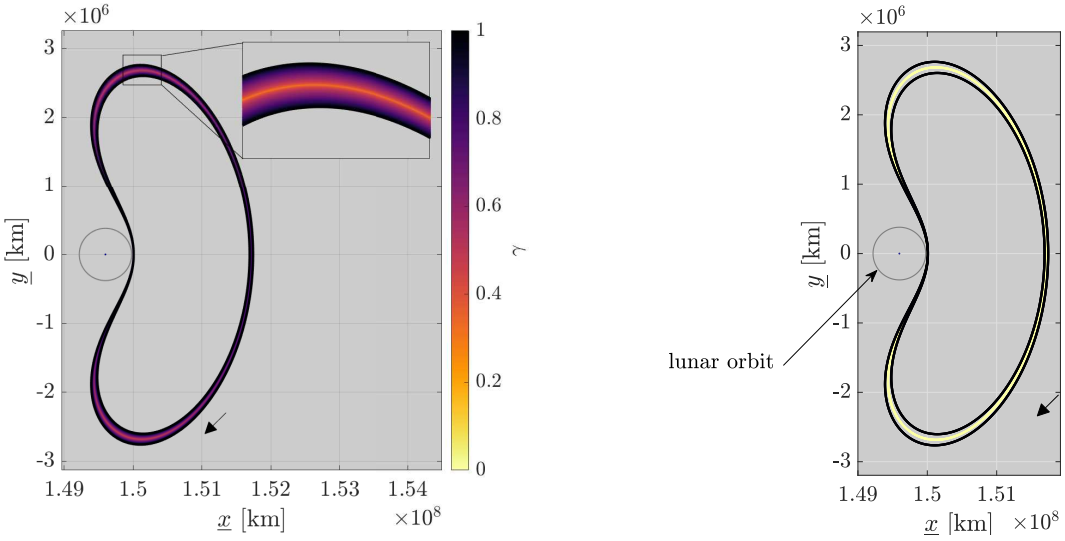

Figure 3. Continuation orbits between the Sun-B_1 CR3BP 2:17 Lyapunov and its BCR4BP periodic counterpart (a). The initial orbit in the CR3BP, in yellow, and the final orbit in the BCR4BP, in black (b).

the southern family members are defined by a negative $\underline{z}$ components. For instance, consider the $\underline{L}_2$ halo family in the Sun-B_1 CR3BP, as plotted in the Sun-B_1 rotating frame in Figure 4(a). The color scale denotes the orbital period, and the darker shades of gray represent the orbits with larger periods. The halo family originates in the $\underline{x}$-$\underline{y}$ plane from the bifurcating orbit in the planar Lyapunov family and evolves out of plane as the family of orbits approaches the secondary body. Recall that in the Sun-B_1 CR3BP, the smaller primary is a fictitious body with mass equal to the sum of the masses of the Earth and the Moon. Thus, the position of the Earth and the orbit of the Moon are indicated for reference in Figure 4(a). Synodic resonant $\underline{L}_2$ halo orbits are selected in the Sun-B_1 CR3BP using a resonance plot.[12,17] A resonance plot, as in Figure 5, represents the ratio of the orbital period to the synodic period versus another parameter, such as the maximum $\underline{z}$ excursion, across a family of periodic orbits. Simple resonance ratios, for instance 1:3 or 2:11 are easily identified in the resonance plot in Figure 5. However, less intuitive ratios, such as 12:73, also yield valid synodic resonant orbits and are identifiable from a resonance plot. The resonance quotients identified in Figure 5 are colored as functions of the type of resonance; 1:α resonances are colored in orange, 2:α resonances in blue, 4:α resonances in green, and other types of resonance, such as 12:73, in purple. Synodic resonant periodic orbits are selected in the Sun-B_1 CR3BP and are then employed as initial guess for the computation of the periodic solutions in the BCR4BP.

The synodic resonant $\underline{L}_2$ halo orbits that are selected from Figure 5 are transitioned from the Sun-B_1 CR3BP to the BCR4BP as formulated in the Sun-B_1 rotating frame. The resulting orbits are plotted along with their CR3BP counterparts in Figure 4(b). Orbits near the $\underline{L}_2$ equilibrium point, for instance the 1:6 or the 12:73 synodic resonant orbits are not significantly perturbed by the actual Earth and the Moon on their respective planetary orbits. In contrast, the $\underline{L}_2$ resonant orbits that pass closer to the Earth and the Moon planetary orbits, such as the 1:3 or the 2:7 synodic resonant halos, visibly differ from the periodic orbits as computed in the Sun-B_1 CR3BP. Note the multiple lobes that are apparent on some of the orbits as computed in the BCR4BP, e.g., the 4:15

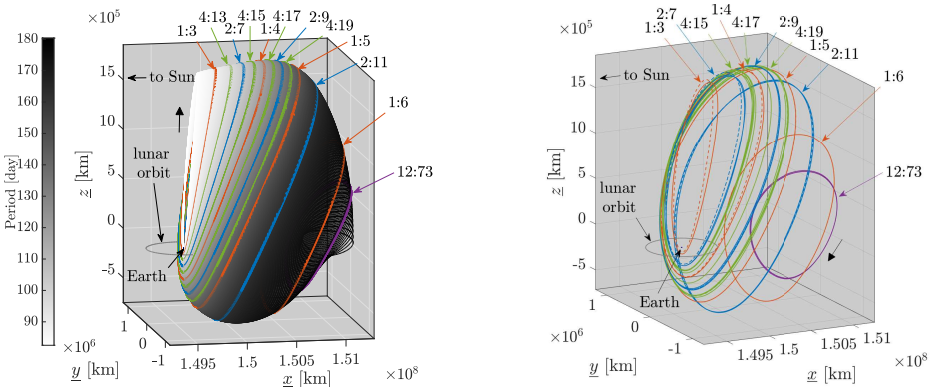

(a) (b)

Figure 4. Representative $\underline{L}_2$ halo orbits, as seen in the Sun-B_1 rotating frame. Selected synodic resonant members are plotted in color. Selected synodic resonant members as computed in the CR3BP, in dashed lines, and in the BCR4BP, in solid lines.

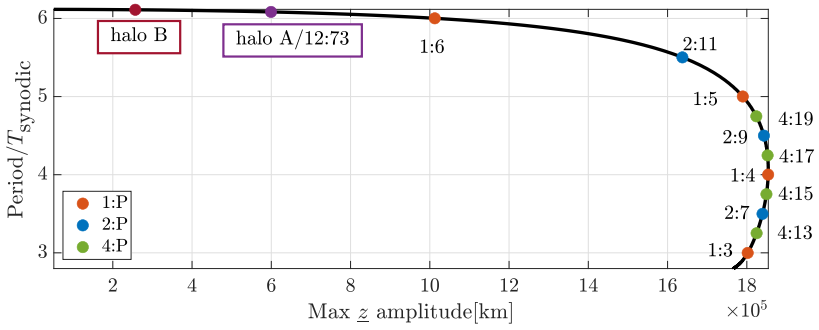

Figure 5. Synodic resonance across a representative subset of the CR3BP Sun-B_1 $\underline{L}_2$ halo family. The $\underline{z}$ amplitude corresponds to the dimension of the orbit when represented in the Sun-B_1 rotating frame.

synodic resonant halo, plotted in green in Figure 4(b). Each lobe corresponds to $^{15}/_4 = 3.75$ synodic periods, or equivalently 3.75 revolutions of the Moon around the Earth-Moon barycenter, B_1. The 12:73 synodic resonant halo orbit includes 12 lobes, but they are indistinguishable at this scale.

Sun-B1 Orbits of Interest

Two synodic resonant BCR4BP halos are considered as destination orbit in this investigation. The Sun-B_1 halo orbit A, plotted in purple in Figure 6, is characterized by similar dimensions as the orbits considered for JWST.[18] The maximum $\underline{z}$ excursion is about 600,000 km and the orbital period is approximately 6 months. This reference halo orbit A corresponds to the 12:73 synodic resonant halo as computed in the BCR4BP and identified in Figure 4(b). The second destination orbit, denoted orbit B, possesses similar dimensions as the baseline orbit for NRST[3] and is plotted in red in Figure 6. The orbital period is nearly 6 months as well (note the apparent asymptote in the left of Figure 5), but the maximum $\underline{z}$ amplitude is equal to approximately 225,000 km. This orbit, denoted by the purple dot in Figure 5, does not correspond to a recognized synodic resonant halo. Thus, it is not strictly periodic in the BCR4BP. However, the orbit is constructed to produced bounded motion for over 2 years; it is accomplished by stacking four revolutions of the orbit and correcting for continuity in the BCR4BP. Note that the JWST and NRST orbit baselines can include

some quasi-periodic motions, representing, for example, Lissajous trajectories[18] or quasihalos. In this investigation, quasiperiodic motion is not currently incorporated in the design process.

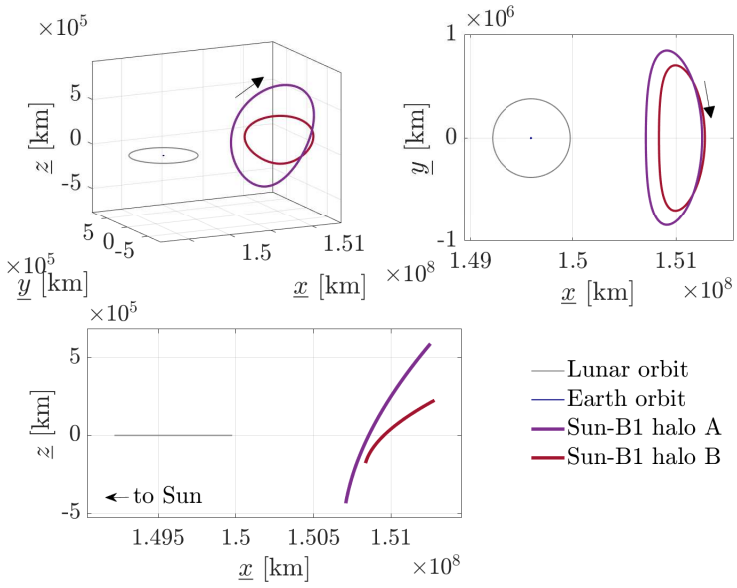

Figure 6. Sample destination orbits in the BCR4BP, as seen in the Sun-B_1 rotating frame

RESULTS

A sampling of transfer trajectories to heliocentric destinations that represent different types of geometries is explored. First, the transfer framework is introduced. Stable manifolds arriving at the two sample destination orbits, the Sun-B_1 halo A and halo B, are propagated backwards in time, and trajectories that encounter the Moon are recorded. Families of trajectories are then produced and summarized in maps. Finally, initial guesses, extracted from the maps, are leveraged to yield end-to-end transfers from the 9:2 synodic resonant NRHO in the Earth-Moon system to heliocentric destination orbits in the BCR4BP. Multiple families of feasible solutions with different geometries are computed and the evolution of the energy along transfers is explored.

Transfer Framework and Invariant Manifolds

Servicing missions from the lunar vicinity to the two sample destination halo orbits are explored in the BCR4BP. Transfers leveraging the natural dynamics to the destination orbit are sought. Thus, manifolds associated with the orbits are leveraged. Manifolds reflect the local flow approaching and departing an unstable periodic orbit and have been exploited previously for interplanetary transfer design.[19,20] While multiple metrics such as various types of stability indices[21,22] exist, the stability (in the linear sense) of a periodic solution is assessed in this investigation using the Lyapunov exponent ϕ_i,[13] that is,

$$\phi_i = \Re\left(\frac{\ln \lambda_i}{\mathbb{P}}\right) \tag{13}$$

where λ_i is the i-th eigenvalue of the monodromy matrix, that is, the state-transition matrix computed for one orbital period, and $\mathbb{P}$ is the orbital period. The necessary condition for linear stability of a periodic orbit is that all the Lyapunov exponents must be equal to zero. One or more nonzero

Lyapunov exponents denote instability and, thus, the existence of approaching and departing flows from the orbit. The Lyapunov exponents across the $\underline{L}_2$ halo family in the Sun-B_1 CR3BP are plotted

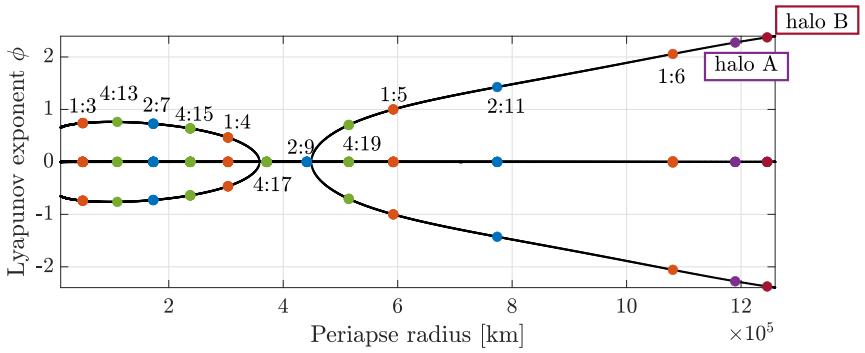

Figure 7. Lyapunov exponents as a function of the periapse distance to the smaller primary across a representative subset of the CR3BP Sun-B_1 $\underline{L}_2$ halo family. Selected synodic resonant halos are plotted as colored dots.

in Figure 7. The periodic $\underline{L}_2$ halos are classified into one of three subsets. Two subsets, for periapse radii between 100,000 and 350,000 km, and between 450,000 and 1,250,000 km, correspond to unstable halo orbits. Finally, the last subset identifies a set of linearly stable orbits, each with a periapse radius between 350,000 and 450,000 km. The resonant synodic orbits that were previously selected are identified by colored dots in Figure 7. The 12:73 synodic resonant halo orbit, i.e., the destination halo orbit A, is unstable in the Sun-B_1 CR3BP, and the Lyapunov exponent associated with the unstable mode has a magnitude equal to 2.2756. The periodic orbit corresponding to halo orbit B is also unstable, with the corresponding Lyapunov exponent equal to ± 2.2815.

The stability characteristics of the two destination halo orbits in the BCR4BP are explored. Both orbits are unstable when computed in the BCR4BP as formulated in the Sun-B_1 frame. The Lyapunov exponents associated with the unstable modes of halo A and halo B are equal to ± 2.3738 and ± 2.3809, respectively. The Lyapunov exponents of both orbits in the CR3BP and the BCR4BP are summarized in Table 1. Thus, the stability properties are maintained when the orbits are transitioned from the Sun-B_1 CR3BP to the BCR4BP as formulated in the Sun-B_1 frame. While the stability properties may vary as the continuation process evolves from the CR3BP to the BCR4BP,[13] both halo orbits remain sufficiently far from the Earth and the Moon that the motion of the Earth and the Moon in their planetary orbits does not severely impact their characteristics. The destination orbits, i.e., the Sun-B_1 halo A and halo B in the BCRB4P, are unstable, and the natural flow along the manifolds is leveraged to access the destination orbit.

Table 1. Lyapunov exponents associated with the destination orbits, as computed in the Sun-B_1 CR3BP and in the BCR4BP as formulated in the Sun-B_1 frame.

	CR3BP			BCR4BP		
Halo A	± 2.2756	0	0	± 2.3738	0	0
Halo B	± 2.2815	0	0	± 2.3809	0	0

Initial Guess Generation

Initial guesses for the transfer from the lunar vicinity to the destination orbits are constructed using manifolds. Stable manifolds approaching the orbits are backwards propagated, and trajectories

that encounter perilune within a sphere of 30,000 km centered on the Moon are recorded. Sample trajectories of different geometries from the manifolds of the halo orbit A are plotted in Figure 8. Three types of geometry are identified. The first type of geometry, colored in orange in Figure 8, encounters an Earth flyby before departing the Earth-Moon system. Note that the Earth flyby helps accomplish part of the inclination change required to reach the Sun-B_1 destination orbit. The second geometry, maroon in Figure 8, corresponds to transfers that exit the Earth-Moon system through the Earth-Moon L_2 gateway. Finally, trajectories plotted in green in Figure 8 encounter a lunar flyby before leaving cislunar space through the Earth-Moon L_2 portal. In general, multiple geometries for transfer trajectories from cislunar space to the Sun-B_1 BCR4BP periodic orbit are efficiently produced from back-propagation of the manifolds associated with the destination orbit.

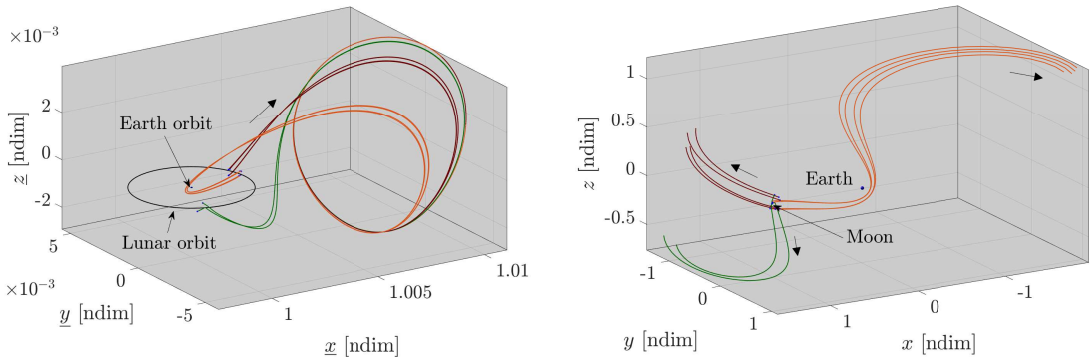

(a) (b)

Figure 8. Sample manifold trajectories from the lunar vicinity to the destination orbit, as viewed in the Sun-B_1 rotating frame (a). Zoomed-in view of the departure from the lunar vicinity, as observed in the Earth-Moon rotating frame (b).

Initial guesses for transfers with a close lunar encounter are of particular interest for various upcoming applications. The proposed Gateway is the current framework for the NASA development of an intermittently crewed space facility near the Moon. From a baseline orbit in a 9:2 synodic resonant Near Rectilinear Halo Orbit (NRHO), the Gateway is intended to serve as proving ground for deep space technologies and as a staging location for missions beyond cislunar space, including potential servicing missions to spacecraft located near the Sun-B_1 collinear libration points. Thus, dynamical structures that naturally link the vicinity of the NRHO to the selected destination orbits are explored within the context of the BCR4BP. A sample stable manifold arc connecting a lunar flyby with the destination orbit is plotted in Figure 9. The 9:2 synodic resonant NRHO is transitioned from the Earth-Moon CR3BP to the BCR4BP as formulated in the Earth-Moon frame[12,13] and is plotted in black. Proximity (in position space) between the manifold arc and the NRHO orbit is apparent. Additionally, the geometry of the trajectory in Figure 9 is consistent with departure flow previously observed in the 9:2 NRHO.[23] Manifold arcs from the Sun-B_1 halo B destination orbit, as computed in the BCR4BP, encounter the 9:2 synodic resonant NRHO and offer transfer opportunities.

Families of Transfers

Families of transfers from the lunar vicinity to the Sun-B_1 libration point region are constructed using favorable stable manifolds from the Sun-B_1 destination halo orbit in the BCR4BP. For each member of the family, the departure state is constrained as a perilune, and an insertion maneuver

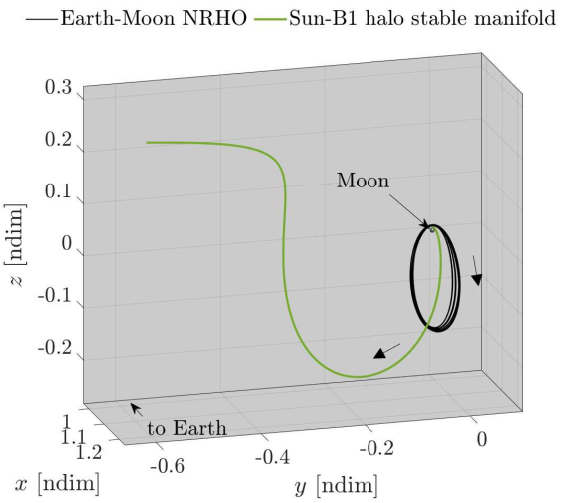

Figure 9. Stable manifold trajectory from the BCR4BP Sun-B_1 halo B destination orbit that encounters the BCR4BP Earth-Moon NRHO, as seen in the Earth-Moon rotating frame.

into the Sun-B_1 arrival orbit is initially allowed. Employing a continuation process, families are then produced in two continuation parameters: departure perilune radius and time of flight. Maps of the resulting transfers appear in Figure 10. The horizontal axis represents the time of flight between the departure state at perilune and the insertion maneuver at the Sun-B_1 orbit. The vertical axis corresponds to the radius from the Moon to the perilune departure state. Each dot corresponds to a converged transfer and is colored by the insertion ΔV cost, using a perceptually uniform color scale.[24] The initial guess from the stable manifold arc associated with the destination halo orbit is plotted as a green dot. Two steps are employed to continue this transfer into families of transfers. First, the time of flight is held constant while the family of transfers is continued in terms of perilune radius. This first family of transfers corresponds to the vertical dark line in Figure 10. Then, families of transfers are continued off this first family. For various selected perilune radii, the corresponding converged transfers in the first family are continued in time of flight, corresponding to the horizontal lines in Figure 10. Using this two-step continuation process, transfers are produced for departure perilune states with radii between 3,000 km and 30,000 km for halo orbit A, and between 3,000 km and 40,000 km for halo orbit B. The times of flight range from approximately 248 to 254 days for transfers to orbit A, and from 265 to 270 days for orbit B. Note the different scales along the color bars between Figures 10(a) and 10(b). Most of the transfers to the Sun-B_1 halo orbit B require an insertion ΔV maneuver of less than 20 m/s. Transfers to the Sun-B_1 halo A with relatively low insertion maneuver cost, i.e., less than 50 m/s, are available for all the sampled perilune radii and for times of flight between 248 and 251 days. These transfers correspond to the points colored in the dark purple shades in Figure 10(a) and correspond to transfers that follow closely the flow into the 12:73 synodic resonant orbit. As the time of flight increases, the insertion ΔV cost increases as well, as denoted by the lighter colored points between 252 and 254 days. Transfers from the lunar vicinity to the Sun-B_1 destination orbit are obtained for relatively low-cost insertion maneuvers.

The range over times of flight in the maps in Figure 10 offer a variety of Earth-Moon-Sun configurations at departure. For instance, consider transfers from a 3,000 km perilune radius to the Sun-B_1 halo A destination orbit. This family of transfers corresponds to the lowest horizontal line in the map in Figure 10(a). The shortest and longest transfers in this family are plotted in Figure 11,

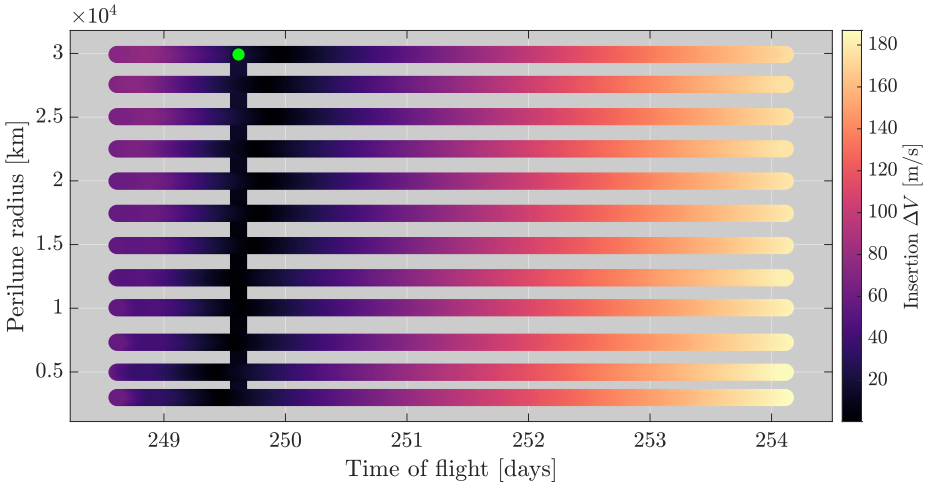

(a) Halo orbit A

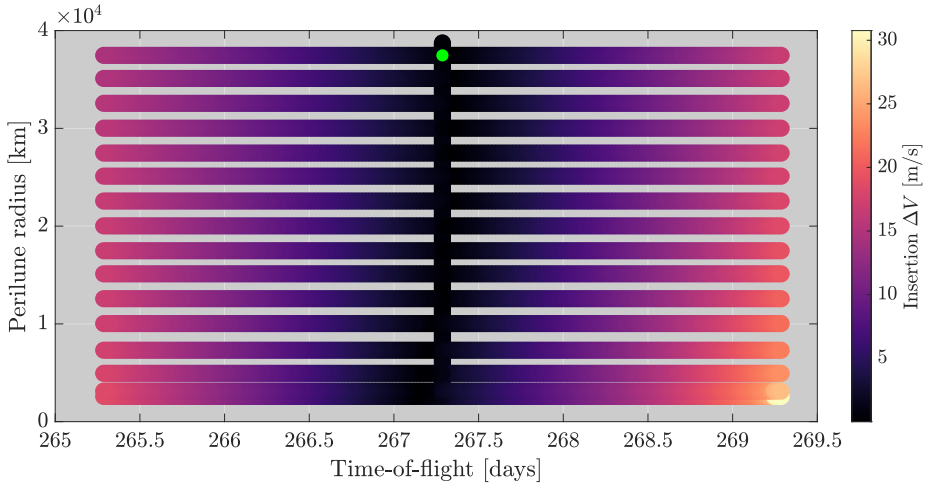

(b) Halo orbit B

Figure 10. Map of transfers from perilune states to the Sun-B_1 destination orbit, colored by the magnitude of the insertion maneuver ΔV. The initial guess from the manifold arc is denoted by a green dot.

as well as the perilune departure states for all of the members of the family. The shortest trajectory, plotted in black in Figure 11, corresponds to a time of flight equal to 248.5 days while the time of flight for the longest transfer, in yellow, approximately equals 254 days. While a difference of 6.5 days in a 250-day transfer appears to be small, the change in the initial relative geometry between the Earth, the Moon and the Sun is not insignificant. Recall that the synodic period, i.e., the period between two consecutive alignments of the Earth, the Sun, and the Moon, is equal to approximately 29.5 days. Thus, the period of the lunar orbit as viewed in the Sun-B_1 rotating frame, plotted in gray in Figure 11, is equal to 29.5 days. By modifying the transfer time of flight, the departure state shifts along the lunar orbit, as observed in Figures 11(a) and 11(b), offering flexibility in the departure epoch. The 6.5-day shift in departure states observed along this family corresponds to nearly one quarter of the synodic period, reflecting a shift in the departure quadrant (note that it is the period of the synodic resonant 9:2 NRHO in the Earth-Moon CR3BP). A set of quadrants, la-

beled I through IV and plotted in Figure 11(b), are defined in the Sun-B_1 rotating frame to facilitate an investigation of the effects of the tidal acceleration[25,26] from the Sun along a given trajectory. This family of transfers represents departure states throughout nearly the entire sector defined for quadrant III. Note that the longest transfer requires a high insertion ΔV, approximately equal to 187 m/s. Thus, while the map supplies a feasible transfer corresponding to this specific epoch and time of flight, additional corrections and/or optimization are necessary to decrease the insertion ΔV.

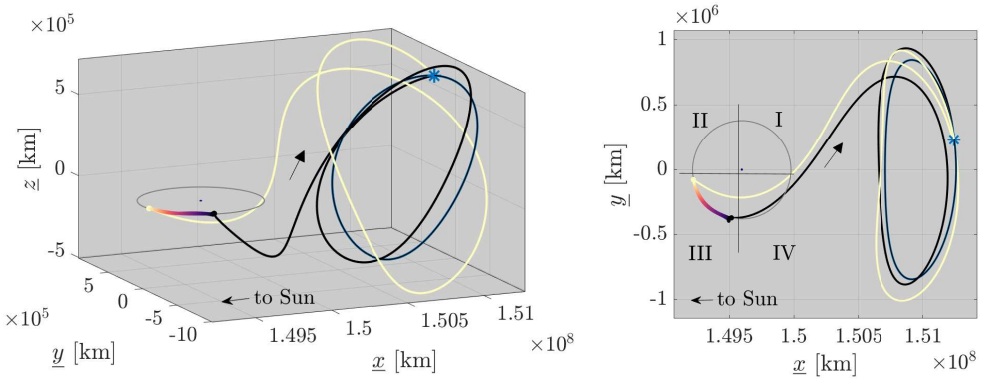

Figure 11. Shortest, in black, and longest, in yellow, transfers from a perilune radius of 3,000 km to the Sun-B_1 halo A. Colored dots denote all the converged transfer departure states with perilune radius equal to 3,000 km, regardless of the time of flight.

Earth-Moon NRHO to Sun-B1 Halo End-to-End Transfers

The maps of converged transfers departing Earth-Moon perilune to the Sun-B_1 halo orbits are leveraged to construct feasible end-to-end transfers from Earth-Moon periodic orbits to the destination orbit. Such transfers are representative of the journey of a potential servicing vehicle. In this example, the departure orbit is the synodic resonant 9:2 BCR4BP NRHO, and the destination orbit is the Sun-B_1 halo orbit B in the BCR4BP. Note that other orbits in the cislunar vicinity, such as Distant Retrograde Orbits (DROs), quasihalo orbits and halo orbits,[3] may be incorporated as departure orbits as well.

Initial guesses for the end-to-end transfer are selected from the map of perilune transfers, in Figure 10(b), given certain parameters. In addition to the insertion ΔV into the destination orbit, the Earth-Moon Hamiltonian values, H, corresponding to the departure states are compared to the Hamiltonian values along the Earth-Moon periodic orbit. Initial guess trajectories that represent the smallest difference in these Hamiltonian values are sought, as they generally yield transfers with small departure maneuvers. For instance, consider the initial guesses for the end-to-end transfers plotted in Figure 12, as viewed in the Earth-Moon rotating frame. Perilune states with Earth-Moon Hamiltonian values that are similar to the 9:2 NRHO are selected and plotted as the colored dots. The transfers associated with these perilune states are plotted in gray. The Hamiltonian values along the 9:2 synodic resonant orbit range from 1693.29 to 1693.31; this range is slightly above the color bar used in Figure 12. The perilunes along transfers with departure energy levels that are similar to the departure NRHO orbit correspond to the darkest dots in Figure 12. In addition to the Hamiltonian value, multiple parameters are relevant when selecting potential transfer from the maps in Figure 10 to seed an initial guess for an end-to-end transfer.

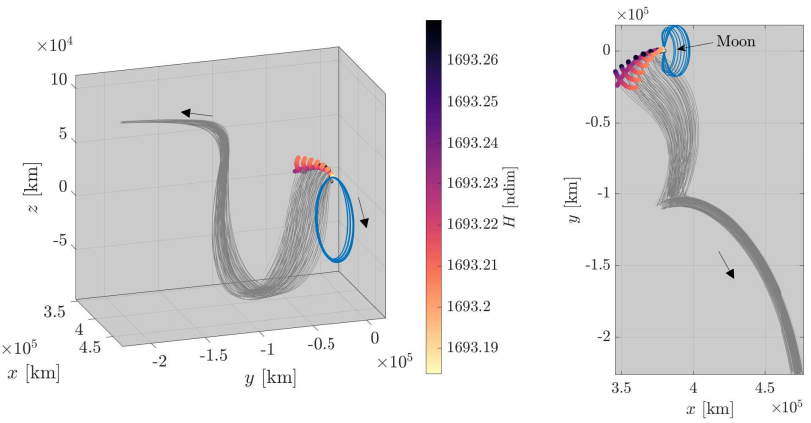

(a) (b)

Figure 12. Selected initial guesses for transfers from the 9:2 synodic resonant NRHO to the Sun-B_1 halo B, as viewed in the Earth-Moon rotating frame. Perilune states are colored by their associated Earth-Moon Hamiltonian values.

A numerical scheme to implement the differential corrections process is employed to produce continuous end-to-end transfers between the departure Earth-Moon orbit and the Sun-B_1 orbit. In this investigation, the differential corrections schemes for the map generation and the transfer construction are applied for states as represented in the Sun-B_1 rotating frame. However, recall that the dynamics in the BCR4BP as described by the equations of motion in the Earth-Moon frame (Equations (4) and (5)) are identical to the behavior modeled by the equations of motion in the Sun-B_1 frame (Equations (8) and (9)). Thus, numerical corrections could also be employed on states represented in the Earth-Moon frame.[27] The initial guess trajectory is discretized into patch points to facilitate the convergence process. While a single-shooting algorithm is an acceptable alternative in certain scenarios, it generally fails for long transfers with close passages of one or more primaries. The transfers in this investigation are characterized by times of flight of over 240 days, and the departure state is located in close proximity (less than 70,000 km) of the Moon. Thus, a multiple-shooting scheme is selected for the numerical corrections. The trajectory is corrected for continuity between consecutive patch points. Maneuvers are allowed at the departure from the NRHO and at the insertion into the Sun-B_1 halo orbit B. The arrival location and epoch in the Sun-B_1 halo orbit are fixed. The time of flight is not explicitly allowed to vary during the corrections process, but is adjusted by modifying the departure location along the Earth-Moon NRHO. Recall that the BCR4BP is a time-dependent, periodic model. Thus, adjusting the departure state also changes the departure time and, thus, modifies the time of flight. Once a transfer satisfies the constraints within some numerical tolerance, families of transfers are obtained by continuing the numerical corrections along some parameter, such as departure location from the NRHO.

End-to-end transfers from the NRHO to the halo B destination orbit are computed for different epochs. Representative transfers in the Sun-B_1 rotating frame are plotted in Figure 13. Trajectories are colored according to the total ΔV, that is, the sum of the departure and arrival maneuver magnitudes. Transfers in Figures 13(a) and 13(b) possess a total ΔV ranging from approximately 90 m/s to 200 m/s, while transfers in Figure 13(c) require a total maneuver cost between 200 m/s and 250 m/s. The insertion ΔV remains consistent across all the transfers, i.e., between 4 and 6 m/s. The majority of the maneuver cost occurs at the NRHO departure: the minimum departure ΔV is approximately 87 m/s for a transfer in Figure 13(b) and the maximum ΔV, about 245 m/s, is pro-

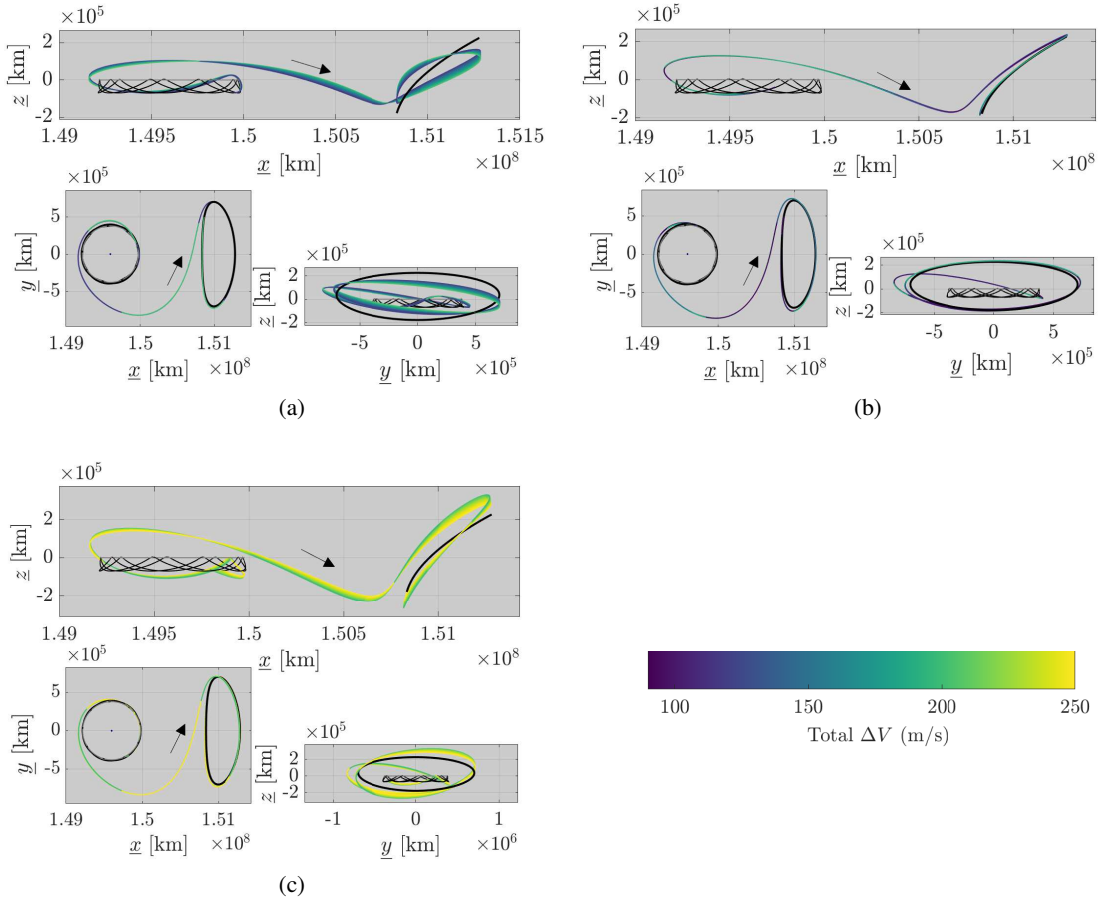

Figure 13. Representative end-to-end transfers between the 9:2 NRHO and the Sun-B_1 halo orbit B, as viewed in the Sun-B_1 rotating frame.

duced for a transfer in Figure 13(c). The initial epoch, i.e., the Earth-Moon-Sun relative geometry at departure, is different for each group of transfers in Figure 13. Recall that, in the BCR4BP, the epoch is described by the Sun angle in the Earth-Moon rotating frame, or, equivalently, the Moon angle and/or the quadrants in the Sun-B_1 frame. Transfers plotted in Figure 13(a) and 13(c) possess departure states from the NRHO as located in quadrant IV. The majority of departure states for the transfers in Figure 13(b) are located in quadrant I and incorporate Moon angles at departures that are similar to the transfers described by Folta and Webster.[3] Note that none of these transfers are optimized. Nevertheless, this investigation demonstrates that natural/low-cost transfers between to cislunar and heliocentric space can be obtained using dynamical systems tools in the BCR4BP.

The geometry of the departure from the Earth-Moon NRHO is explored. Close views of the previous transfers in Figure 13 are now plotted in the Earth-Moon rotating frame in Figure 14. The maneuver to depart from the NRHO is constrained to occur to near apolune. Near perilune, higher dynamical sensitivity and higher orbit determination errors present challenges to obtain consistent departures. However, note the difference in the departure location from the NRHO: transfers in Figures 14(a) and 14(c) include departure maneuvers prior to apolune, while transfers in Figure 14(b) depart from the NRHO after perilune. All transfers present this sharp 'turn', indicated by the red arrows in Figure 14 in space after leaving the NRHO. This geometry is consistent with

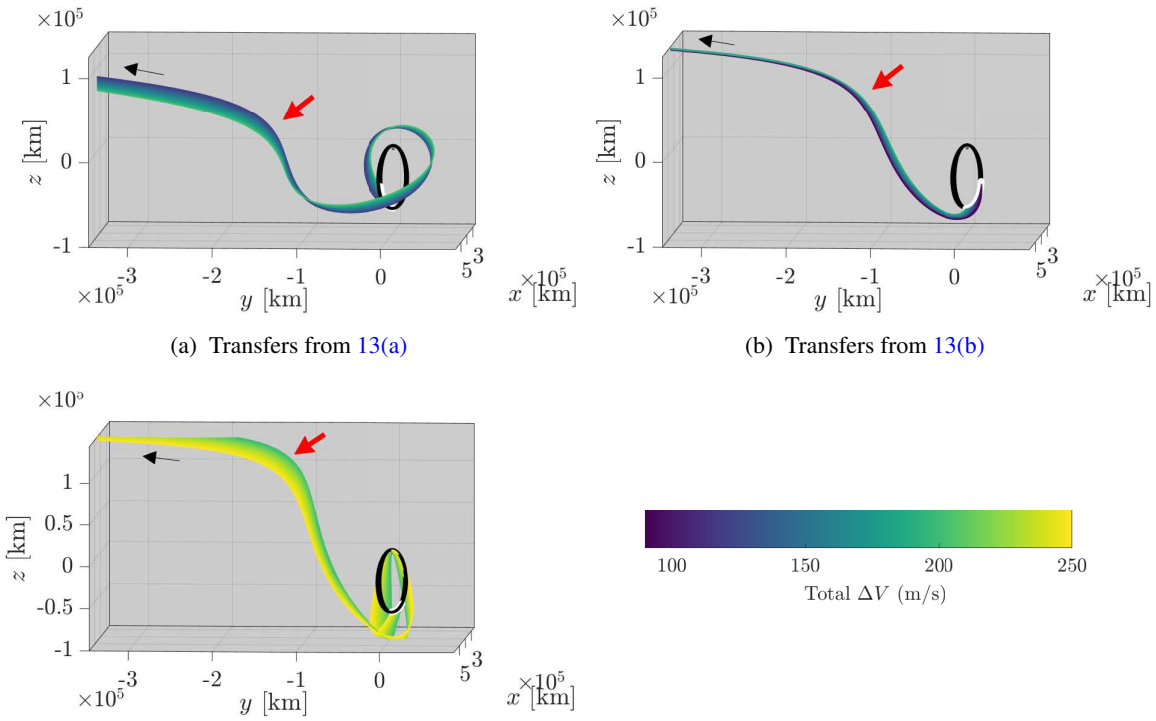

(a) Transfers from 13(a)

(b) Transfers from 13(b)

(c) Transfers from 13(c)

Figure 14. NRHO departure geometry from the end-to-end transfers in Figure 13, as viewed in the Earth-Moon rotating frame. The departure maneuver locations are denoted by white dots.

observations from previous contributions:[23] departure arcs from the NRHO that do not present this 'turn' do not have sufficient energy to depart the Sun-B_1 portals. The numbers of loops around the Moon differ for each type of transfer plotted in Figure 14: no loop around the Moon for the transfers in Figure 14(b), one loop for the transfers in Figure 14(a), and two loops for the transfers in Figure 14(c). Note that the close lunar flybys in trajectories in Figure 14(c) could cause some navigation challenges, and that some of the trajectories intersect the lunar radius.

Table 2. Range of the characteristics associated with the transfers plotted in Figures 13 and 14

	Transfers (a)	Transfers (b)	Transfers (c)
Dep. ΔV [m/s]	117.0 : 202.2	87.4 : 187.4	196.9 : 245.1
Arr. ΔV [m/s]	5.3 : 5.4	4.7 : 4.8	4.5 : 4.6
Total ΔV [m/s]	**122.3 : 207.6**	**92.1 : 192.1**	**201.4 : 249.7**
Time of flight [days]	271.2 : 273.3	263.0 : 265.4	274.5 : 275.9
Dep. Moon angle [deg]	-30.5 : -4.8	66.2 : 95.4	-61.8 : -45.6

Energy Considerations

The evolution of the energy along the NRHO-to-halo transfers is explored. Recall that the BCR4BP does not admit an integral of the motion. Two time-dependent Hamiltonian values, the Earth-Moon Hamiltonian value H and the Sun-B_1 Hamiltonian value $\underline{H}$, are defined to be the

energy-like quantities in the BCR4BP. The Earth-Moon Hamiltonian values along the transfers in Figure 13(b) are plotted as a function of the Moon angle $\underline{\theta}$ in Figure 15. The Hamiltonian values associated with the Earth-Moon 9:2 NRHO are plotted in black. The states of the Sun-B_1 halo orbit are rotated into the Earth-Moon rotating frame; the associated Earth-Moon Hamiltonian values are plotted in red in Figure 15. Note the differences in the Hamiltonian value oscillations between the two periodic orbits. The oscillations along the red line are much larger than those along the black line, since the dimensions of the halo orbit B are larger when represented in the Earth-Moon rotating frame. The oscillations along the red line also have a lower frequency due to the longer orbital period of halo B as compared to the NRHO, represented in black. The Hamiltonian values associated with the transfers in Figures 13(b) and 14(b), depicted in the blue to purple colors in Figure 15, accomplish naturally the required change of energy between the Earth-Moon NRHO and the Sun-B_1 halo orbit A. A small discontinuity in Hamiltonian values are present at departure

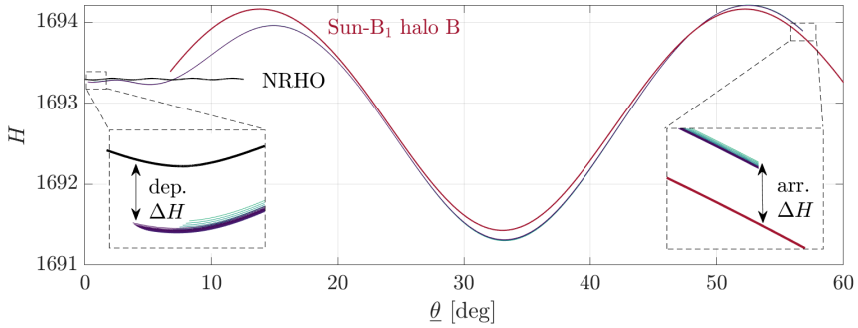

Figure 15. Earth-Moon Hamiltonian values along the transfers in Figure 13(b);Hamiltonian values associated with the Earth-Moon NRHO and the Sun-B_1 halo orbit B are plotted in black and in red, respectively.

between the transfer arc and the NRHO, and at arrival between the transfer arc and the Sun-B_1 halo orbit, as illustrated in the insets in Figure 15. These differences are labeled the departure ΔH and the arrival ΔH, and correspond to the minimum ΔV maneuver required to achieve this change of energy, assuming the velocity vector of the incoming/outgoing transfer arc and the velocity vector of the insertion/departure location in the periodic orbit are aligned. A larger maneuver is required if the directions of the velocity vectors are not aligned. The angle between the transfer arc velocity vector and the velocity vector along the periodic orbit, Λ, is defined

$$\Lambda = \arccos \frac{\bar{v}_{\text{t}} \cdot \bar{v}_{\text{p.o.}}}{\|\bar{v}_{\text{t}}\| \|\bar{v}_{\text{p.o.}}\|} \tag{14}$$

where $\bar{v}_{\text{t}}$ and $\bar{v}_{\text{p.o.}}$ are the velocity vectors along the transfer arcs and the periodic orbit, respectively. For Λ equal 0°, the maneuver is tangential to the periodic orbit velocity vector and maximizes the change in energy. Conversely, for Λ equal 90°, the maneuver direction and the velocity vector along the periodic orbit are perpendicular, the maneuver minimizes the change in energy. The Λ angles at the departure from the NRHO for transfers in Figures 13(b) and Figure 14(b) are plotted as a function of the z component of the departure location in Figure 16(a). Transfers near apolune possess a Λ angle between 50° and 70°, and thus, the associated maneuvers do not efficiently change the Hamiltonian value. As a consequence, the total ΔV for these transfers is relatively high, between 160 and 190 m/s. In contrast, the Λ angle for departure locations with z component between -55,000 km and -38,000 km possess a Λ angle between 10° and 15°. The maneuvers from these locations are close to tangential to the periodic orbit, and the total ΔV is between 90 and 110 m/s. Note that

the theoretical minimum ΔV[28] maneuvers between the Earth-Moon NRHO and the Sun-B1 halo B stable manifold range from 40 m/s to 85 m/s, depending on the departure location along the NRHO. Additional numerical corrections processes could potentially further decrease these value of Λ and thus, the total ΔVs associated with the transfers. The majority of the energy change required in the transfer between the Earth-Moon NRHO and the Sun-B_1 halo orbit occurs with the natural dynamics of the Earth-Moon-Sun system, and the effectiveness of the departure and insertion maneuvers is assessed using the Λ angle.

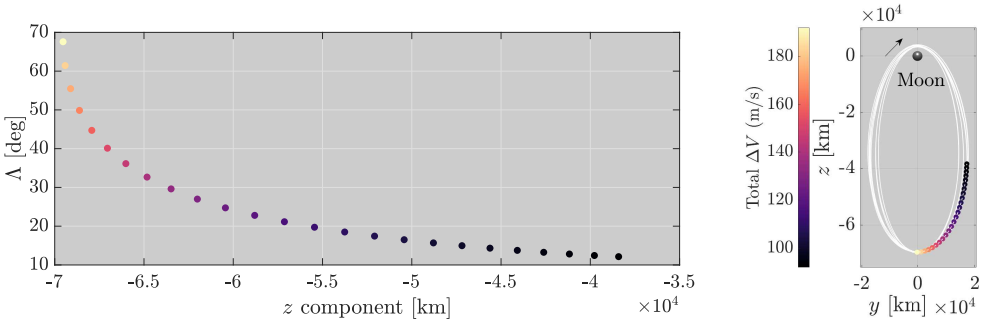

(a) (b)

Figure 16. Λ angle at departure from the Earth-Moon NRHO associated with the transfers in Figures 13(b) and 14(b) (a). Departure locations along the Earth-Moon NRHO, as viewed in the Earth-Moon rotating frame (b).

CONCLUDING REMARKS

With the upcoming James Webb Space Telescope and the Nancy Roman Space Telescope, opportunities for servicing missions between cislunar space and heliocentric space will arise in the near future. This investigation aims to demonstrate that a framework for designing such transfers can be created within the Earth-Moon-Sun BCR4BP. A method to transition a synodic resonant orbit from the Sun-B_1 CR3BP to the BCR4BP as formulated in the Sun-B_1 rotating frame is introduced. The stable manifolds associated with Sun-B_1 BCR4BP halo orbits are leveraged to construct transfers that naturally encounter the Moon. Families of transfers from the different perilune radii are computed, and maps corresponding to these families are leveraged to select initial conditions for end-to-end transfers from an Earth-Moon orbit to a Sun-B_1 orbit. As an application, multiple families of transfers between the Earth-Moon 9:2 synodic resonant BCR4BP NRHO and a Sun-B_1 BCR4BP halo orbit are computed. The transfers represent a range of departure epochs and a variety of geometries for the NRHO departure. An analysis of the Earth-Moon Hamiltonian value, an energy-like quantity in the BCR4BP, confirms that the transfers leverage natural Earth-Moon-Sun dynamics, and the effectiveness of the departure and insertion maneuvers is assessed.

ACKNOWLEDGMENTS

This work was conducted at Purdue University and NASA Johnson Space Center under contract number NNJ13HA01C with additional effort under cooperative agreement NNX13AK60A and grant #80NSSC18M0122. The authors thank the members of the Purdue Multi-Body Dynamics Research Group for useful discussions. Also acknowledged is the Purdue University School of Aeronautics and Astronautics for facilities and support, including access to the Rune and Barbara Eliasen Visualization Laboratory.

REFERENCES

[1] S. Ross and M. Lo, "The Lunar L1 Gateway - Portal to the Stars and Beyond," *AIAA Space 2001 Conference and Exposition*, Albuquerque, New Mexico, 2001.

[2] D. E. Lee, "White Paper: Gateway Destination Orbit Model: A Continuous 15 Year NRHO Reference Trajectory," tech. rep., NASA, 2019.

[3] D. C. Folta and C. Webster, "Transfer Trajectory Options for Servicing Sun-Earth-Moon Libration Point Missions," *AAS/AIAA Astrodynamics Specialist Conference*, Portland, Maine, 2019.

[4] V. G. Szebehely, *Theory of Orbits, the Restricted Problem of Three Bodies*. Academic Press, 1967.

[5] G. Gómez, J. Llibre, R. Martínez, and C. Simó, *Dynamics And Mission Design Near Libration Points - Vol II: Fundamentals: The Case Of Triangular Libration Points*. World Scientific Monograph Series In Mathematics, World Scientific Publishing Company, 2001, 10.1142/4402.

[6] M. Jorba-Cuscó, A. Farrés, and A. Jorba, "Two Periodic Models for the Earth-Moon System," *Frontiers in Applied Mathematics and Statistics*, Vol. 4, 2018, p. 32.

[7] K. K. Boudad, *Disposal Dynamics From The Vicinity Of Near Rectilinear Halo Orbits In The Earth-Moon-Sun System*. M.S. Thesis, Purdue University, West Lafayette, Indiana, 2018.

[8] M. A. Andreu, *The Quasi-Bicircular Problem*. Ph.D. Dissertation, Universitat de Barcelona, Barcelona, Spain, 1998.

[9] K. C. Howell, "Families of Orbits in the Vicinity of the Collinear Libration Points," *Journal of the Astronautical Sciences*, Vol. 49, 1998, 10.2514/6.1998-4465.

[10] D. J. Grebow, *Generating Periodic Orbits in the Circular Restricted Three-Body Problem with Applications to Lunar South Pole Coverage*. M.S. Thesis, Purdue University, West Lafayette, Indiana, 2006.

[11] R. A. Broucke, "Stability of Periodic Orbits in the Elliptic, Restricted Three-Body Problem," *AIAA Journal*, 1969, 10.2514/3.5267.

[12] K. K. Boudad, D. C. Davis, and K. C. Howell, "Near Rectilinear Halo Orbits in Cislunar Space within the Context of the Bicircular Four-Body Problem," *2nd IAA/AAS SciTech Forum*, Moscow, Russia, 2019.

[13] K. K. Boudad, D. C. Davis, and K. C. Howell, "Dynamics of Synodic Resonant Near Rectilinear Halo Orbits in the Bicircular Four-Body Problem," *Advances in Space Research*, Vol. 66, Nov. 2020, pp. 2194–2214, https://doi.org/10.1016/j.asr.2020.07.044.

[14] H. J. Pernicka, *The Numerical Determination of Nominal Libration Point Trajectories and Development of a Station-Keeping Strategy*. Ph.D. Dissertation, Purdue University, West Lafayette, Indiana, 1990.

[15] H. B. Keller, *Solution of Two Point Boundary Value Problems*. AAS/AIAA Astrodynamics Specialist Conference, Society for Industrial and Applied Mathematics, 1976.

[16] K. C. Howell, "Three-Dimensional, Periodic, 'Halo' Orbits," *Celestial Mechanics*, Vol. 21, No. 1, 1984, pp. 53–71.

[17] E. M. Zimovan, K. C. Howell, and D. C. Davis, "Near Rectilinear Halo Orbits and their Application in Cis-Lunar Space," *3rd International Academy of Astronautics Conference on Dynamics and Control of Space Systems*, Moscow, Russia, 2017.

[18] "James Webb Space Telescope User Documentation," https://jwst-docs.stsci.edu/jwst-observatory-hardware/jwst-orbit, May 2017.

[19] W. Koon, M. Lo, J. Marsden, and S. Ross, *Dynamical Systems, the Three-Body Problem and Space Mission Design*. Interdisciplinary Applied Mathematics, Springer New York, 2006.

[20] M. Kakoi, *Design of Transfers from Earth-Moon L1/L2 libration point orbits to a destination object*. M.S. Thesis, Purdue University, West Lafayette, Indiana, 2012.

[21] N. Bosanac, *Exploring the Influence of a Three-Body Interaction Added to the Gravitational Potential Function in the Circular Restricted Three-Body Problem: a Numerical Frequency Analysys*. M.S. Thesis, Purdue University, 2012.

[22] E. M. Zimovan-Spreen, K. C. Howell, and D. C. Davis, "Near Rectilinear Halo Orbits and Nearby Higher-Period Dynamical Structures: Orbital Stability and Resonance Properties," *Celestial Mechanics and Dynamical Astronomy*, 2020.

[23] D. C. Davis, K. K. Boudad, R. J. Power, K. C. Howell, and D. J. Sweeney, "Heliocentric Escape and Lunar Impact from Near Rectilinear Halo Orbits," *AAS/AIAA Astrodynamics Specialist Conference*, Portland, Maine, 2019.

[24] S. v. d. Walt and N. Smith, "mpl colormaps," https://bids.github.io/colormap/.

[25] D. C. Davis, *Multi-Body Trajectory Design Strategies Based on Periapsis Poincaré Maps*. Ph.D. Dissertation, Purdue University, West Lafayette, Indiana, 2011.

[26] D. C. Davis and K. C. Howell, "Characterization of Trajectories Near the Smaller Primary in the Restricted Problem for Applications," *Journal of Guidance, Control, and Dynamics*, Vol. 35, No. 1, 2012, pp. 116–128.

[27] S. T. Scheuerle, B. P. McCarthy, and K. C. Howell, "Construction of Ballistic Lunar Transfers Leveraging Dynamical Systems Techniques," *AAS/AIAA Astrodynamics Specialist Conference*, Lake Tahoe, California, 2020.

[28] A. D. Cox, *Transfers to a Gravitational Saddle Point: An Extended Mission Design Option for LISA Pathfinder*. M.S. Thesis, Purdue University, West Lafayette, Indiana, 2016.